Renewable and Sustainable Energy Reviews 159 (2022) 112093

Contents lists available at ScienceDirect

Renewable and Sustainable Energy Reviews

journal homepage: www.elsevier.com/locate/rser

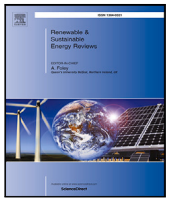

Energy management system for a hybrid PV-Wind-Tidal-Battery-based islanded DC microgrid: Modeling and experimental validation

Muhammad Fahad Zia [a,*], Mashood Nasir [b], Elhoussin Elbouchikhi [c], Mohamed Benbouzid [a,d], Juan C. Vasquez [b], Josep M. Guerrero [b]

[a] University of Brest, UMR CNRS 6027 IRDL, 29238 Brest, France
[b] Department of Energy Technology, Aalborg University, 9220 Aalborg, Denmark
[c] ISEN Yncréa Ouest, LabISEN, 29200 Brest, France
[d] Shanghai Maritime University, Logistics Engineering College, 201306 Shanghai, China

ARTICLE INFO

Keywords:
DC microgrid, Tidal energy, Battery degradation, Energy management system, Optimization

ABSTRACT

DC microgrids are becoming integral part of a modern power system due to the growing penetration of DC distributed energy resources and loads, with additional advantages in terms of power quality improvement. They can be used for remote area electrification including villages, mountains, and islands. In this paper, an islanded DC microgrid is considered as a case study for islands with tidal energy potential, which consists of renewable energy resources including solar, wind and tidal, along with Li-ion battery storage. To ensure the efficient operation, an optimal energy management system is proposed for resource scheduling and utilization. In this regard, this paper proposes a two-stage supervisory energy management system for optimal operation of PV/Wind/Tidal microgrid with one-time communication to avoid excessive use of communication bandwidth in real-time. The primary stage schedules the optimal energy share from each energy source thereby enhancing the efficiency of the operation. The secondary stage updates the decision strategies by analyzing aggregated scheduled generation and demand profiles to ensure an effective utilization. The proposed energy management model has been experimentally validated to prove its effectiveness in achieving optimized operation for an islanded DC microgrid. Word Count: 4380

1. Introduction

Distributed energy resources (DERs) are changing the paradigm of future electric power system. Indeed, they are being used for providing electricity to both on- and off-grid areas with large share of renewable energy sources (RESs). RESs have become integral part of future power system for ensuring both environmental protection and sustainability [1]. They are being used to provide electricity to remote off-grid areas due to the advantage of being installed in the proximity of load ends. However, RESs produce intermittent power, which can be overcome by using energy storage systems (ESSs) and demand response [2]. Due to solar PV DC generation, DC battery storage and advent of DC/DC power electronics converter and DC distribution technologies, DC loads have been deeply penetrated in residential and commercial sectors [3,4]. Hence, with ESSs, DC RESs, and increased use of DC loads, DC microgrids (MGs) are being regarded as the key solution for hard-to-reach energy users [5–7]. In the literature, DC MGs have used various types of RESs. It involves exploring PV and battery system potentials [7,8], wind turbines [9], wave energy systems [10], and tidal turbines [11,12] for meeting electric energy demands.

MGs suffer from control and coordination problems originated from inter-temporal operation of ESSs and intermittent nature of RESs. In this regard, an energy management system (EMS) is required to mitigate these issues and optimizing the MG energy management operation over long duration [13]. MG energy management system performs optimal scheduling of MG system against defined objectives in the domains of economics, environment, and reliability among others [14–16]. EMS is the tertiary layer of MG control and in hierarchy it operates above the control and power management levels, i.e above primary and secondary layers respectively [17]. Control level ensures voltage and current regulation, while power management level deals with harmonic compensation, line limits, and voltage and frequency restoration. Therefore, EMS layer ensures operational efficiency while also governing lower layers of control to satisfy the system stability and performance requirements.

* Corresponding author.
E-mail addresses: muhammadfahad.zia@univ-brest.fr, fahad.zia@nu.edu.pk (M.F. Zia).

https://doi.org/10.1016/j.rser.2022.112093
Received 30 November 2020; Received in revised form 28 June 2021; Accepted 9 January 2022
Available online 5 February 2022
1364-0321/

A nonlinear multivariable and coordinated energy management strategy is developed in [18] for proportional power sharing in islanded DC MG system, which normally converges to a local optimum solution and may be time consuming and inefficient [19]. In [20], the dynamic performance of AC and DC buses are comparatively analyzed for grid-connected residential MG with hybrid ESS integration. In [21], an economic cost model is used for optimal management of MG DERs. A heuristic approach is presented in [11] for managing operation of a hybrid renewables-based MG in an islanded context, which seems to be non-optimal. In [22], the real-time stochastic power management strategies have been reviewed, which ensure smooth operation of hybrid renewable energy systems. A bi-objective EMS model is developed in [23] for optimal operation of an islanded DC MG with improved small signal stability performance. However, these EMSs are not validated on the experimental level or hardware-in-loop platforms.

In experimentally verified EMSs for islanded DC MGs, a dynamic optimization model is developed in [24] for power sharing among DERs. However, it does not consider battery degradation cost for having longer battery lifetime. In [25], a non-optimal EMS is proposed for preventing state of charge (SOC) violations of hybrid ESSs in islanded DC MG system. A simplified modeling of PV and storage-based islanded MG is experimentally validated in [26], which does not include an optimization model for cost-effective MG operation. Rule-based EMSs are presented in [27] and [28] for non-optimal operation of islanded DC MGs. In [29], a predictive EMS is proposed for preventing or reducing outage duration in PV and battery-powered islanded DC MG, but optimal load shedding model is ignored. Similarly, a non-optimal state machine control is developed in [30]. A sub-optimal hierarchical EMS is presented in [31] for minimizing hydrogen consumption of a hybrid PV, battery and fuel cell powered islanded DC MG.

Most of the aforementioned EMSs have not proposed an optimization model for an effective operation of the islanded DC MG system. These EMSs continuously share information with local controllers in real-time and massive communication expenditures happen in real-time for these EMSs. Moreover, the aforementioned EMSs do not consider the potentials of tidal energy for remote islands applications. The practical battery degradation cost model is also ignored. Furthermore, they have not considered the optimal scheduling taking into account the battery lifetime degradation. In our previous work [32], an optimal EMS is experimentally validated, however, it does not include load shedding and battery cyclelife limitations. Moreover, EMS strategy for low generation periods is not considered. Contrariwise, this paper considers not only the EMS with optimal resource scheduling but also considers the battery degradation cost. The mathematical formulation of the EMS optimization model is generic in nature and can be applied to other MGs as well.

Fig. 1 shows an off-grid DC MG with PV panels, battery, wind and tidal turbines, along with power electronic interface for each renewable energy resource and battery storage system integration. The power electronic interface mainly consists of power electronic converters where AC/DC converters are used for the DC bus integration of turbines (wind and tidal). In order to have close resemblance of real case load demand, a DC/DC converter is used for constant power load profile generation. Besides, PV and battery are also integrated in DC MG using dedicated DC/DC converters. An EMS is used for supervisory control of DC MG. EMS performs the operation of data collection, where it stores the data of load demand, resource availability, etc. EMS collects and stores data from energy sources and load to perform future forecasting and system analysis. EMS also performs scheduling operation in two stages (optimization and adjustment), where it efficiently determines a day-ahead schedule of all energy sources. Lastly, EMS acts as a coordinator for information exchange to local controller. All local controllers of RESs operate in either MPPT or power curtailment modes.

The rest of the paper is structured as follows: the EMS stage and its mathematical modeling are discussed in Section 2; the local controllers strategies are explained in Section 3; Section 4 presents the hardware-in-loop experimentation platform and results, while based on the results, conclusions are drawn in Section 5.

2. Energy management system

The energy management system determines a day-ahead optimal decision strategies for efficient energy utilization in a DC MG system. The hardware-in-the-loop setup used for DC MG system emulation and EMS implementation is presented in Fig. 2. The proposed EMS is formulated in two stages: optimization and adjustment stages. In the first stage, forecasted generation and load profiles, operating costs and penalty data, DERs operational limits, and DC MG system data are sent to the optimization model for determining decision strategies. These scheduled strategies are then sent to the adjustment stage. The adjusted day-ahead scheduled decisions are forwarded to local controllers, which do not communicate with EMS in real-time in order to prevent excessive use of communication bandwidth and avoid security threats in real-time. The EMS stages are presented in detail in the following.

2.1. Optimization stage

The proposed energy management problem for DC MG is mathematically modeled using mixed-integer linear programming (MILP) formulation. The generic form of mixed-integer linear programming is [33],

$$\begin{aligned}
&\min \quad f(y) = c_0 + \sum_{k=1}^{p} c_k y_k \\
&\text{subject to:} \\
&G(y) \le a \\
&H(y) = b \\
&y_i \in \mathbb{R}, \qquad i = 1, 2, \ldots, n \\
&y_j \in \{0, 1\}, \quad j = 1, 2, \ldots, m
\end{aligned} \tag{1}$$

where, y are the decision variables containing both real, y_i, and binary decision variables, y_j. $f(y)$ is an objective function, comprising of real and binary decision variables with $p = m + n$. $G(y)$ and $H(y)$ are inequality and equality constraints, respectively, which define the feasible region in which the optimal solution must have to lie.

In the proposed technique for optimal energy management, a binary variable is assigned with the charging/discharging state of the battery. The remaining decision variables are the real numbers. The overall time scale for operation is defined as T, and the sampling interval is defined as Δt to have $N = T/\Delta t$ discrete time slots. K shows the sample time intervals and may vary from 1 to N, i.e. $K = \{1, 2, 3, \ldots, N\}$. The equality and inequality constraints for the proposed optimization model along with the key objective are modeled in terms of mixed-integer linear programming as can be seen below:

$$\begin{aligned}
\min \quad f = \sum_{k \in K} \Bigg\{ & C_k^b \left(\eta^+ P_k^{b+} + \frac{P_k^{b-}}{\eta^-} \right) \\
& + \sum_{x \in X} \zeta^x \left(P_{f,k}^x - P_k^x \right) + C^{ls} P_k^{ls} \Bigg\} \Delta t
\end{aligned} \tag{2}$$

$$C_k^b = \frac{1}{2} \frac{\left[C_{inv}^b + \sum_{i=1}^{n} C_{om}^b (1+r)^{-i} \right] (1+r)^n - RV}{(1+r)^n \chi_{T_k}^E \chi_{T_k}^Y \chi_d^Y Y_{ref} E_{ref}} \tag{3}$$

$$0 \le P_k^x \le P_{f,k}^x, \quad x \in X, k \in K \tag{4}$$

$$0 \le P_k^{b+} \le \delta_k P_{max}^b, \quad k \in K \tag{5}$$

$$0 \le P_k^{b-} \le (1 - \delta_k) P_{max}^b, \quad k \in K \tag{6}$$

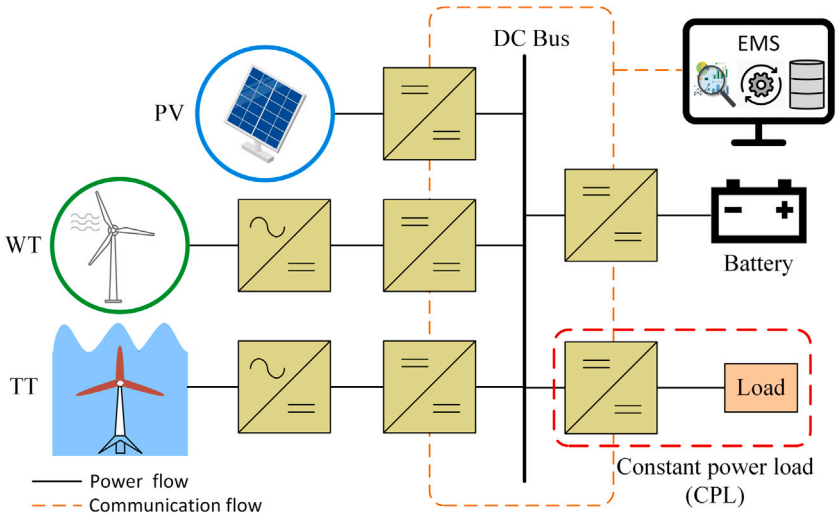

Fig. 1. Islanded DC MG architecture.

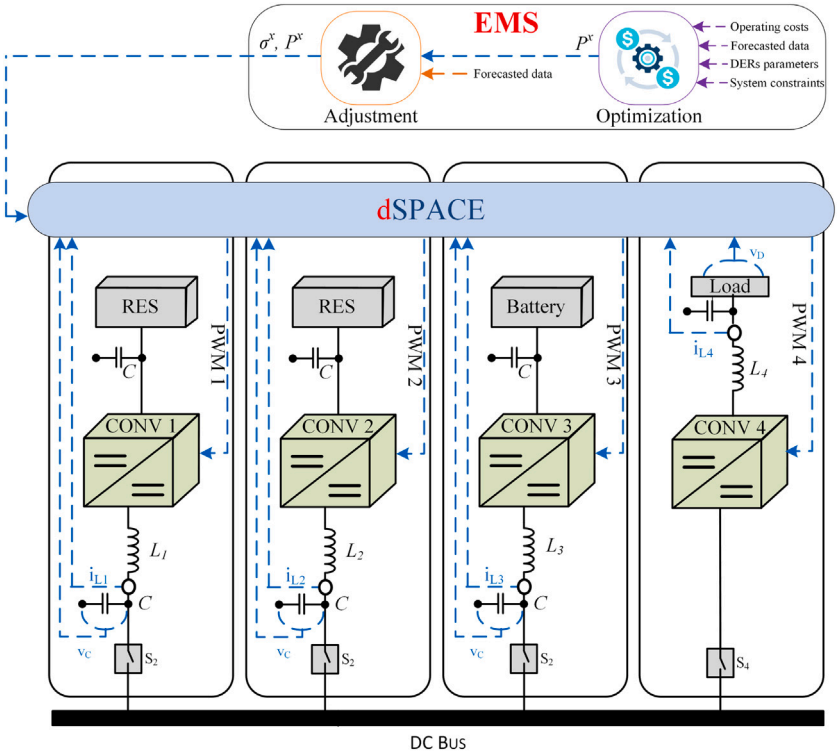

Fig. 2. Hardware-in-the-loop DC microgrid setup scheme.

$$SOC_k = SOC_{k-1} + \frac{1}{E_r^b}\left[\eta P_k^{b+} - \frac{P_k^{b-}}{\eta}\right]\Delta t,\ k \in K \tag{7}$$

$$SOC_{min} \le SOC_k \le SOC_{max},\quad k \in K \tag{8}$$

$$SOC_N \ge SOC_{th} \tag{9}$$

$$0 \le P_k^{ls} \le P_t^d,\quad k \in K \tag{10}$$

$$\sum_{x \in X} P_k^x - P_k^{b+} + P_k^{b-} = (1+\alpha)P_k^d - P_k^{ls},\quad k \in K \tag{11}$$

$$\delta_k \in \{0,1\},\quad k \in K \tag{12}$$

The objective function is shown in Eq. (2) that corresponds to the minimization of the total operating cost in the proposed system. C_k^b models the degradation cost for the Li-ion battery at the intervals k. ζ^x is defined as a penalization cost for each RES. C^{ls} is the penalization cost on load shedding. P_k^{b+} and P_k^{b-} denotes the power for battery charging and discharging at index k, respectively. η shows the full-trip efficiency of the Li-ion battery. P_k^x is the decision variable for the power produced by a RES x at index k, while $P_{f,k}^x$ is its forecasted power. The set X presents the typology of RESs; PV, wind, and tidal energy. P_k^{ls} is the decision variable for load shedding at index k. The battery degradation cost, C_k^b, is modeled in (3) using temperature and depth of discharge-dependent power fading and capacity fading coefficients. C_{inv}^b is the investment cost and C_{om}^b, operation and maintenance cost with discount rate, r. RV represents the residual value, while Y_{ref} and

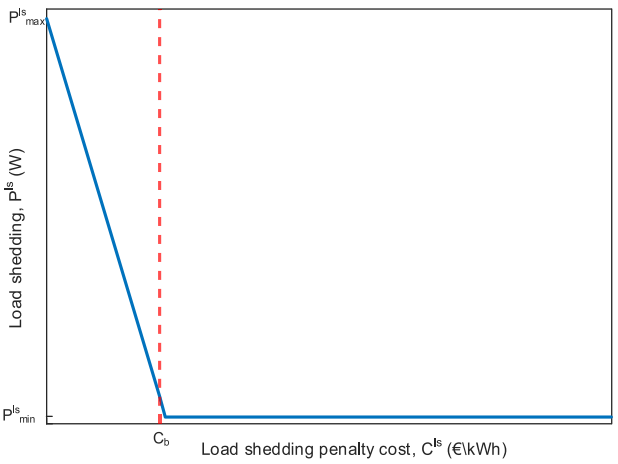

Fig. 3. Impact of penalization cost on load shedding.

E_{ref} is the referenced cyclelife and energy capacity of battery, respectively. χ_d^Y, $\chi_{T_k}^E$, and $\chi_{T_k}^Y$ are depth of discharge-dependent cyclelife, and temperature-dependent energy capacity fading and cyclelife coefficients respectively. They are obtained from the practical regression models of battery degradation developed in [34].

Eqs. (4)–(12) represents the EMS optimization model constraints. Constraint (4) makes sure power from each RES is within the allowable thresholds as forecasted. Constraints (5) and (6) makes sure that at any time interval k battery either charges or discharges. The battery dynamic SOC representation is modeled in (7). Constraint (8) ensures that the battery SOC remains within its defined minimum, SOC_{min}, and maximum, SOC_{max}, limits. Constraint (9) ensures that the battery final SOC should always be the same or more than the defined SOC threshold SOC_{th}, which is defined by the EMS operator based on the history of operational statistics of the islanded DC MG system. Constraint (10) defines P_k^{ls} as a non-negative decision variable whose value cannot exceed the total power demand, P_k^d, at instant k. Constraint (11) makes sure that power is balanced in the MG system, where α corresponds to the losses in the system on the base of cumulative power demand. As discussed, the charging and discharging state variable is presented in (12).

The value of ζ^x should be selected such that it ensures maximum utilization of available generated power of all RESs. The proposed EMS model shall not ensure maximum utilization of RESs generated power in case of ζ^x being less than battery degradation cost C^b. Hence, the battery shall minimally charge and discharge to achieve overall minimum operating cost for islanded DC MG with power balancing. Therefore, ζ^x should be selected such that it always have greater penalization value as compared to C_k^b at any instant k. However, it may create problems of higher charge–discharge cycles consumption, thus reducing battery lifespan. Hence, Eq. (13) is proposed for restricting maximum use of number of battery charge–discharge cycles, n_Θ^b, over the scheduling period. d is the depth of discharge of battery, which is equal to $d = SOC_{max} - SOC_{min}$. The EMS operator determines the battery cycle limit using historical operation data of the islanded DC MG system.

$$\sum_{k\in K}\left[\eta^+ P_k^{b+} - \frac{P_k^{b-}}{\eta^-}\right]\Delta t \le n_\Theta^b E_r^b d \tag{13}$$

Therefore, the proposed EMS model for an islanded DC MG is modified as:

$$\begin{aligned}&\min \quad f\\ &\text{subject to} \quad (4)\text{–}(13)\end{aligned} \tag{14}$$

Algorithm 1 EMS adjustment stage strategy for RESs local controllers

Input: $P_k^x, \alpha, P_k^d \ \forall x,k$
Initialization: $\sigma_k^x = 0 \ \forall x,k, PD = 0, PG = 0$
1: $PD \leftarrow \sum_{k\in K} P_k^d$
2: $PG \leftarrow \sum_{k\in K}\sum_{x\in X} P_k^x$
3: **for** $k \leftarrow 1, \mathrm{N}$ **do**
4: **if** $PG < (1+\alpha)PD$ **and** $SOC_k < SOC_{max}$ **then**
5: $\sigma_k^x \leftarrow 1 \ \forall x$
6: **else**
7: $\sigma_k^x \leftarrow 0 \ \forall x$
8: **end if**
9: **end for**
Output: $\sigma_k^x, P_k^x \ \forall x,k$

The penalization cost on load shedding C^{ls}, defined in the objective function $f(y)$, should be greater than both of ζ^x and C_k^b at each instant k to avoid unnecessary load shedding. The load shedding penalization cost should be higher than battery degradation cost, as shown in Fig. 3, to avoid undesirable load shedding. Load shedding shall be more in case of higher battery degradation cost because the optimization stage must have to ensure minimum operating cost of islanded DC MG. Participation of battery shall be low due to its higher degradation cost as compared to load shedding cost. As load shedding cost becomes more than battery degradation cost, minimum load shedding will happen. Hence, penalization costs and battery degradation costs are selected in the order of $C^{ls} \ge \zeta^x > C_k^b$ for effectively achieving optimal results from the proposed EMS model. This islanded DC MG-EMS model is solved by mixed-integer linear programming solver of YALMIP toolbox in MATLAB [35].

2.2. Adjustment stage

The centralized EMS, in addition to high utilization of communication bandwidth, faces security threat due to constant data and information sharing with the central controller. In this regard, a modified communication strategy is proposed for information sharing among local controllers and EMS. An EMS collects data from all participants only one time for data analytics and scheduling optimization. Once the EMS performs optimization, the modified decisions are communicated to other participants only once to maximally avoid security threats and use minimum communication bandwidth in real-time.

The scheduling decisions of the EMS optimization model are modified using the proposed efficient EMS strategy presented in algorithm 1. In this stage, EMS compares aggregated day-ahead demand and scheduled decisions of RESs. If aggregated demand and system losses are more than the total scheduled generation, the EMS sends scheduled optimal decisions to all local controllers of RESs, P_k^x, and information of auxiliary variable, σ_k^x. This auxiliary variable informs RESs local controllers in algorithm 2 to provide maximum power by using the MPPT mode at each instant k. In case of total power generation being more than demand and losses, RESs have to operate in the power limitation mode. Since battery storage primarily regulates the DC bus voltage, it will keep on charging or discharging within allowable limits of charge–discharge cycles. The daily charge–discharge cycles value is defined such that it ensures continuous real-time operation of the DC MG system.

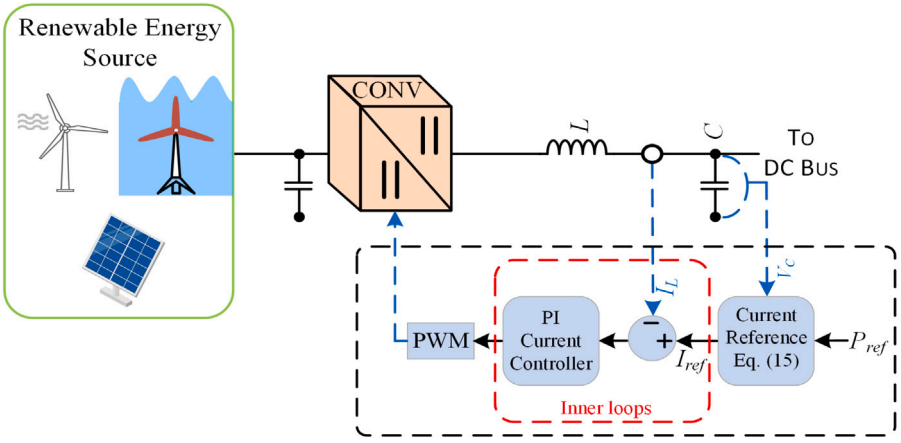

Fig. 4. Power control loops for RESs.

Algorithm 2 Selecting operation mode for RESs

Input: $P^x_{MPPT}, P^x_k, \sigma^x_k \; \forall x, k$
Initialization: $P^x_{ref} = 0 \; \forall x$
1: **for** $k \leftarrow 1, \mathrm{N}$ **do**
2: **if** $\sigma^x_k = 1$ **then**
3: $P^x_{ref} \leftarrow P^x_{MPPT} \; \forall x$
4: **else if** $P^x_{MPPT} < P^x_k$ **then**
5: $P^x_{ref} \leftarrow P^x_{MPPT} \; \forall x$
6: **else**
7: $P^x_{ref} \leftarrow P^x_k \; \forall x$
8: **end if**
9: **end for**
Output: $P^x_{ref} \; \forall x$

3. Local controllers

3.1. RESs controller

This paper focuses on the islanded operation of DC MG system. Hence, the local controllers of all RESs follow the power references provided by the EMS. The unified implementation of these local controllers is presented in Fig. 4, where the inner current control loop regulates the current injected into the DC MG system. The current control loop is preceded by a current reference generator to provide a feed-forward reference current signal, I_{ref}, which is determined through active power reference, P_{ref}, and the output voltage of each RES, V, and it is given as:

$$P_{ref} = V \; I_{ref} \tag{15}$$

The operating modes of RESs are the decision strategies of EMS, which are calculated using the results of the proposed optimization scheme. Therefore, all RESs either generate maximum power or curtail power generation as decided by EMS. However, in case if the power produced by REs is lower than the reference determined by EMS, a simplified algorithm 2, selects minimum of the scheduled power and MPPT power as a reference. MPPT algorithms are beyond the scope of this paper. However, MPPT strategies for PV, wind turbine and tidal turbine generators are extensively discussed in Refs. [36–39] for interested readers.

3.2. Battery controller

A bi-directional DC–DC converter is employed to control the charging and discharging of the Li-ion battery. Moreover, it also acts as a grid-forming converter with battery flexibility at its input side. Therefore, battery not only balances the power differences, but also tends to stabilize the DC bus voltage through the bidirectional converter. The Coulomb counting method is used to calculate the state of the charge (SOC) for the battery [40,41], as given by

$$SOC(t) = SOC_0 + \frac{1}{C_b} \int I_b dt \tag{16}$$

where, $SOC(t)$ is battery SOC at time t and SOC_0 is its initial state. I_b is the current drawn from or given by the battery. C_b is the battery rated capacity.

A dual loop V–I controller is used for the control of bidirectional converter [42] as can be seen in Fig. 5. The inner current loop generates the reference for the outer voltage loop and the outer voltage loop regulates the DC bus voltage, $V_{B,ref}$. The voltage loop PI controller output must be limited to generate current reference within the specified charge (discharge) current limits of the battery. Hence, $I_{b,max}$ represents the maximum limit of charge (discharge) current of the battery. This means that the battery provides power to the DC MG until it reaches its maximum discharge current limit, after which it provides constant power. The same scenario happens in case of charging when battery takes power from the DC MG system.

4. Case study and experimental results

4.1. Setup description

An off-grid DC MG consisting of PV-wind-tidal and Li-ion battery is used as a case study for Ouessant island in Bretagne region in France [11]. The hardware-in-the-loop (HIL) experimental setup has been implemented using Danfoss converters and dSPACE RTI 1006 platform at the DC Microgrid Research Laboratory in Aalborg University, which is shown in Fig. 6. The HIL platform consists in four power electronic converters where the first one is used to emulate PV, second one is used to emulate wind turbine (WT), and tidal turbine (TT), third one is used to emulate battery, and the last one is used to emulate constant power load (CPL). The power control of the fourth converter allows the generation of desired load profile. Various parameters of the HIL system are given in Table 1. The penalization cost of each RES and load shedding are taken as 1 €/kWh and 2 €/kWh, respectively. Initial SOC of battery is taken as 70%. The battery degradation cost is obtained using temperature profile and battery investment and operation costs data from [6].

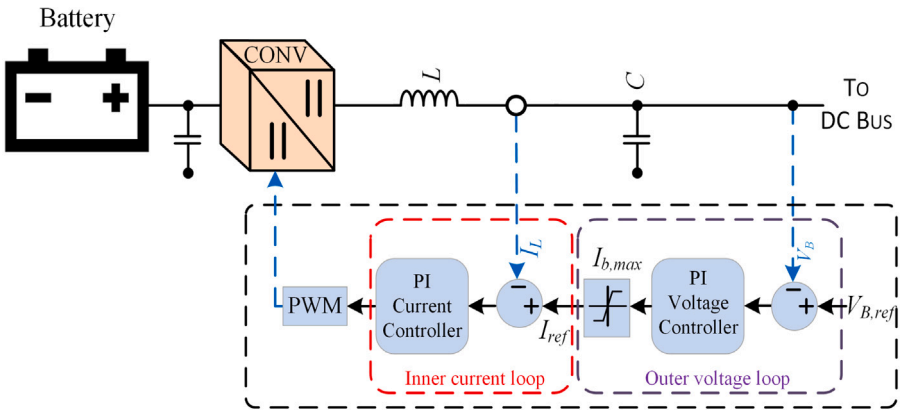

Fig. 5. Inner current and outer voltage control loops for battery.

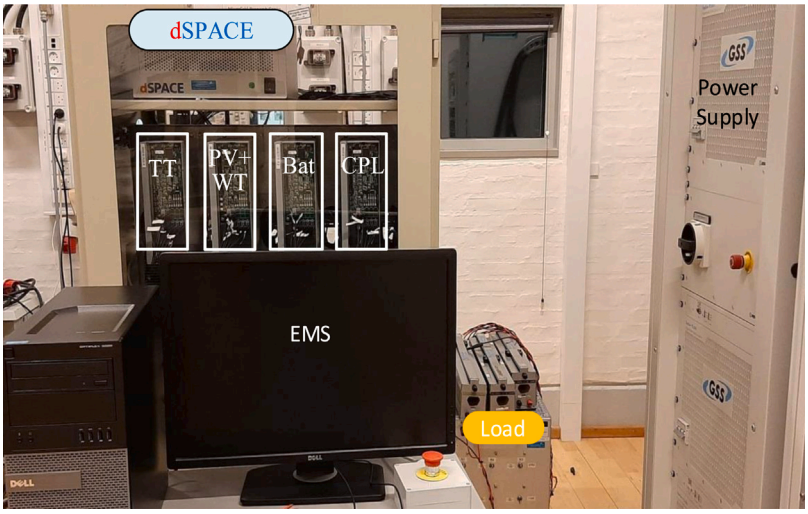

Fig. 6. Experimental setup of the islanded DC MG.

Table 1
System parameters of the islanded DC MG.

Parameters	Value
DC bus nominal voltage	380 V
Battery rated capacity	20 kWh
Maximum charge (discharge) power	2 kW
Battery round-trip efficiency	0.95
Maximum SOC	80%
Minimum SOC	30%
Threshold SOC	50%
Sampling frequency	10 kHz
Inverter inductor	1.8 mH
DC bus capacitance	3.3 mF
Current loop proportional gain	0.005
Current loop integral gain	0.5
Voltage loop proportional gain	0.62
Voltage loop integral gain	0.06
Load	33 Ω

The PV, wind, tidal, and load power profiles of Ouessant island are taken from [6,11] for one day operation and values are scaled for the purpose of experimental validation. The system losses are considered as 5% of the load demand. The EMS optimization model considers sampling time equal to 1 h for 24 h scheduling horizon, thus takes 24 discrete time indices. The prediction errors in PV power, wind power, tidal power, and load demand are taken as 5% of their forecasted values. All local controllers are running in real-time and the scheduling profiles are scaled from hours to seconds (1 h: 60 s) for experimental validation. Two cases have been considered for analyzing the effectiveness of the proposed EMS in terms of adjustment stage, battery storage system operation in different scenarios, and representation of load shedding:

- **Case A:** Power produced by RESs is more than the total forecasted load demand.
- **Case B:** Power produced by RESs is less than the total forecasted load demand.

4.2. Case A

The experimental results for case A are presented in Figs. 7 to 11, which show profiles of RESs, battery, demand, and DC bus voltage for case A. Fig. 7 presents both forecasted and real-time load demand. Load shedding does not happen as power production of RESs and battery power are enough to meet the real-time load demand. Figs. 8 and 9 graphically represent the MPPT and real-time power production of RESs. The power of RESs is curtailed when load demand is not high and battery has either high SOC capacity or it can be charged later in case of high power availability following the decision strategies of the EMS. Hence, RESs local controllers follow the scheduled power and operate in power limitation mode when needed.

The battery charge (discharge) power and SOC profiles are presented in Fig. 10. Battery is charging when RESs generate more power than load and it is discharging when power generation of RESs is less than the load demand and real-time losses. As RESs produce more

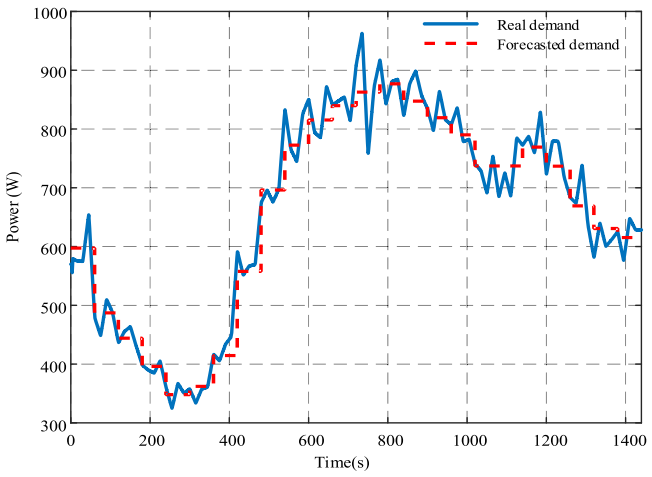

Fig. 7. Real and forecasted power demand profiles (case A).

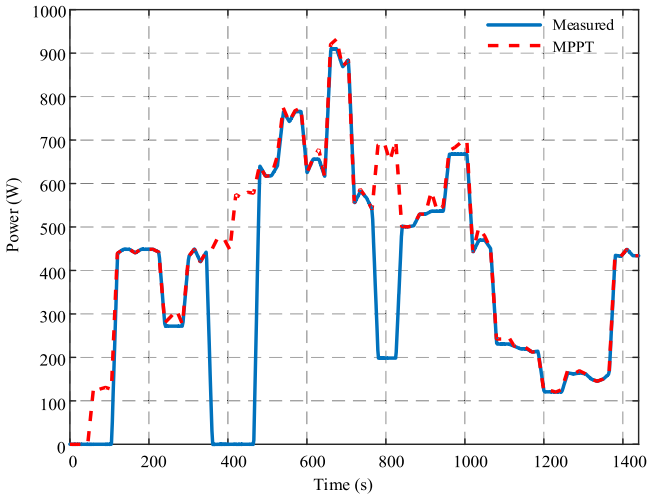

Fig. 8. Measured and MPPT power profiles of combined PV and WT (case A).

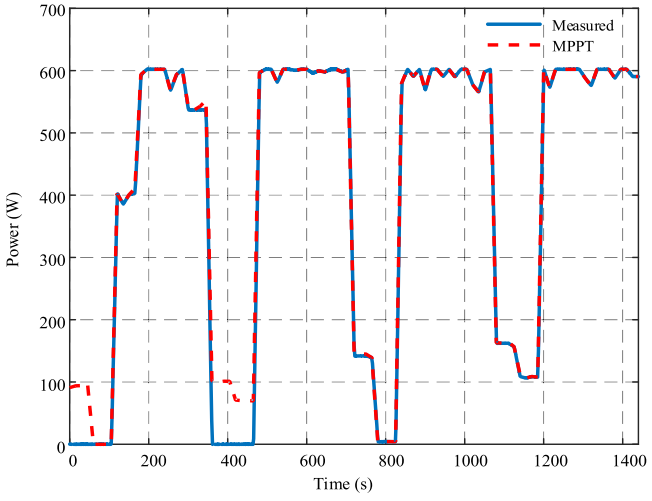

Fig. 9. Measured and MPPT power profiles of TT (case A).

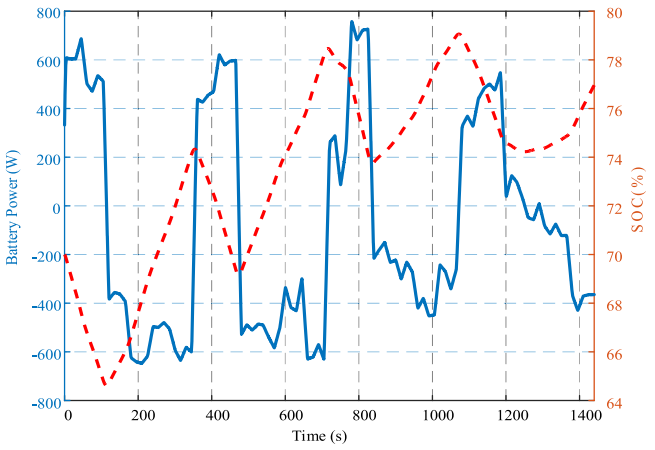

Fig. 10. Battery power and SOC profile (case A).

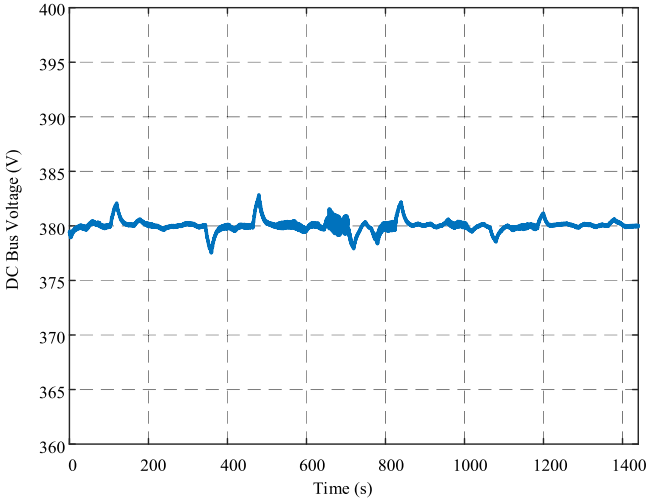

Fig. 11. DC bus voltage (case A).

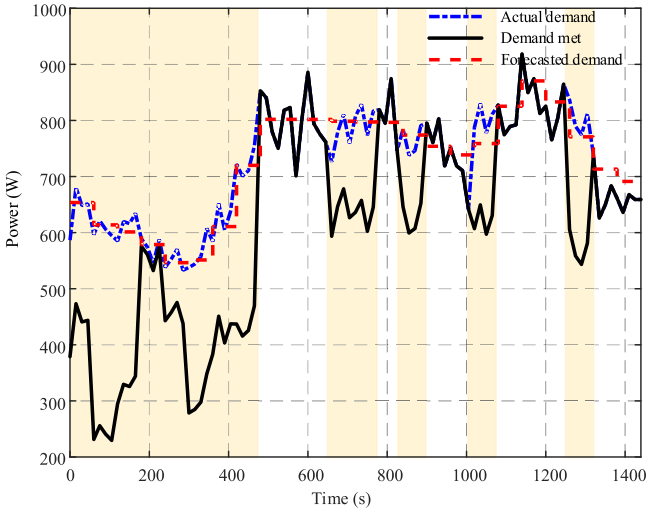

Fig. 12. Real and forecasted power demand profiles (case B).

power than the required load demand, the final state of battery SOC is higher than its initial state. Fig. 11 shows the DC bus voltage profile, which always stays close to the referenced DC bus voltage of 380 V. Small high and low spikes are observed, when battery has to regulate bus voltage with sudden changes in RESs produced power or abrupt increase in load demand. However, the bus voltage profile clearly

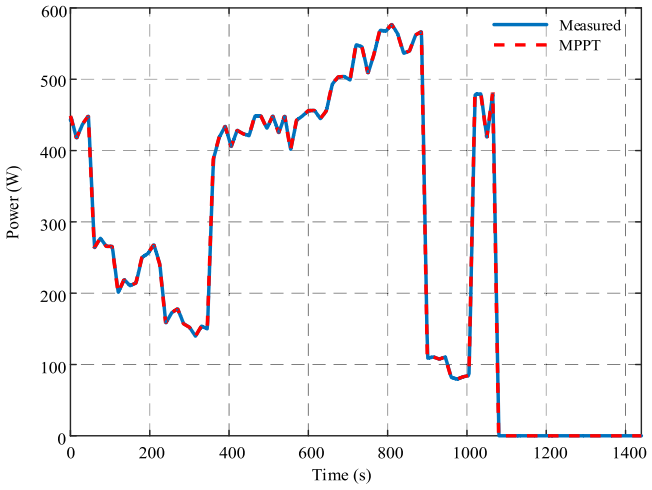

Fig. 13. Measured and MPPT power profiles of combined PV and WT (case B).

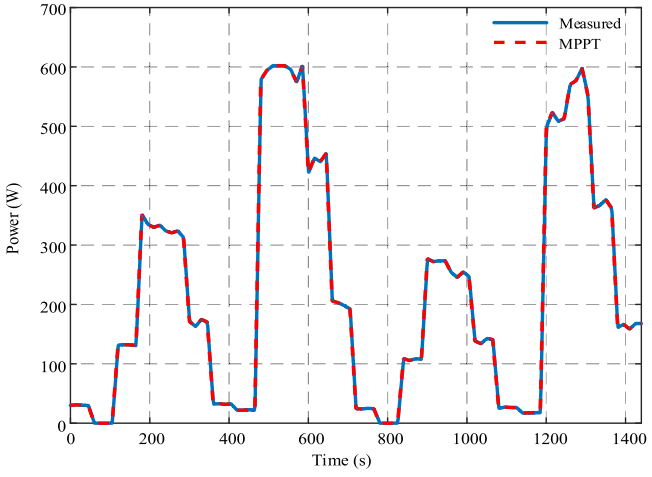

Fig. 14. Measured and MPPT power profiles of TT (case B).

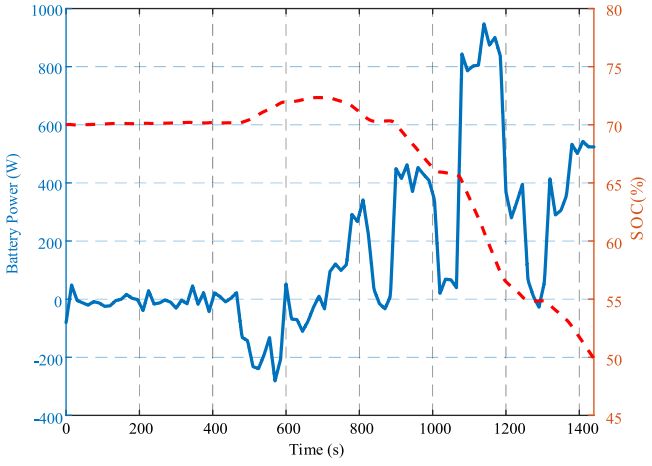

Fig. 15. Battery power and SOC profile (case B).

shows that it always remains within the voltage stability margins of ±5% of the referenced DC bus voltage, which proves that the islanded DC MG is performing stable operation.

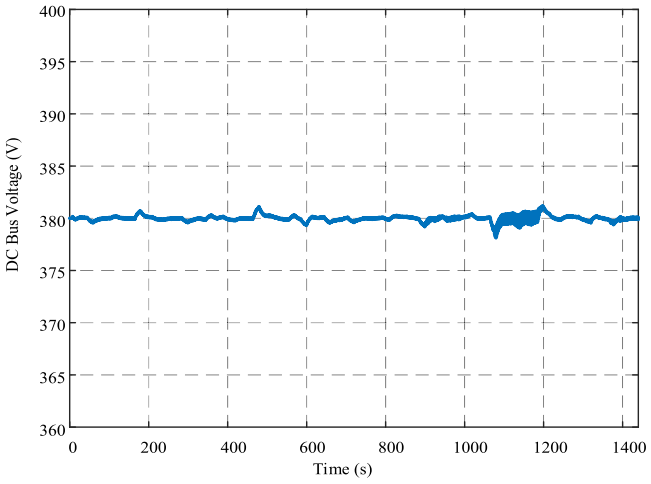

Fig. 16. DC bus voltage (case B).

Table 2
Comparison of proposed EMS performance.

	Real	MILP EMS (stage-I)		Proposed EMS	
	cost ($)	Estimated cost ($)	Gap (%)	Estimated cost ($)	Gap (%)
Case A	2.173	2.377	9.388	2.188	0.690
Case B	5.283	5.438	2.934	5.242	0.776

4.3. Case B

The experimental results for case B are presented in Figs. 12 to 16. In this case, RESs are not able to generate enough power to meet load demand. Hence, load shedding happens whose decision has been forwarded by the EMS to the CPL converter that performs load shedding at the initial stage. The yellow shaded region represent load shedding in Fig. 12, where the met actual demand is presented by solid line. However, all loads must be disconnected in case of no control on the load, and the EMS optimization model will be modified by introducing integer decision variable in place of continuous decision variable for load shedding [43]. Moreover, all local controllers of RESs follow the EMS strategy to operate in MPPT mode, which is also validated by Figs. 13 and 14. Fig. 15 shows that battery is constantly discharging to provide power for achieving real-time supply demand balance and regulating DC bus voltage at the referenced value. Fig. 16 shows that DC bus voltage almost remains constant at its referenced value of 380 V despite having small fluctuations in voltage profile.

4.4. Proposed EMS performance

The proposed performance EMS for islanded DC MG can be evaluated by the daily operating cost gap criterion, which has been defined as follows:

$$\text{cost gap} = \frac{|\text{real operating cost - estimated operating cost}|}{\text{real operating cost}} \quad (17)$$

Table 2 presents comparison between MILP EMS (stage-I) and proposed EMS. The cost gap in proposed EMS is less than 1% as compared to MILP EMS. Hence, the results validate that the proposed EMS approach for islanded DC MG provides better approximation of operating cost as compared to MILP EMS and it can be effectively used for better islanded DC MG scheduling.

4.5. Impact of initial and threshold SOCs

The initial and threshold (final) SOCs play an important role in determining scheduled strategies for renewable-based DC MG operation

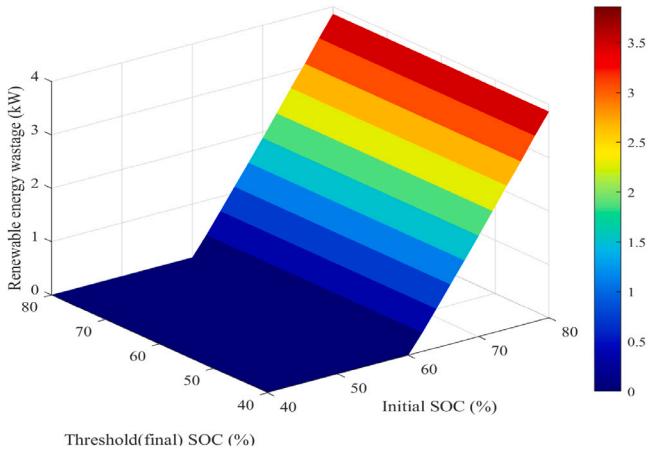

Fig. 17. Impact of initial and threshold SOCs on renewable energy wastage (case A).

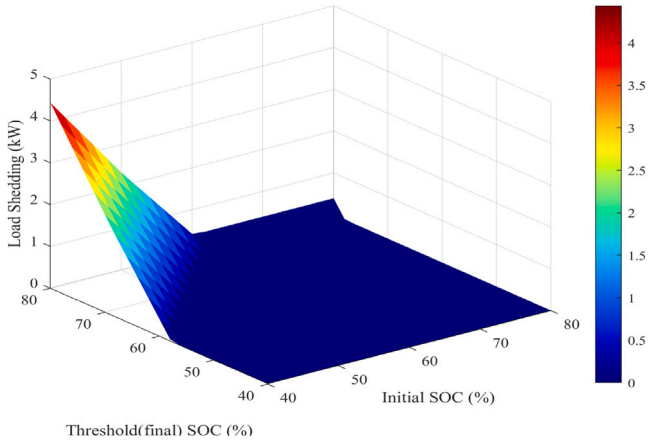

Fig. 18. Impact of initial and threshold SOCs on load shedding (case A).

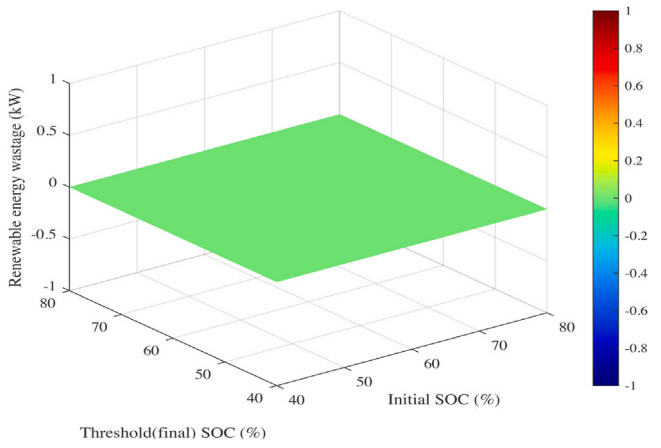

Fig. 19. Impact of initial and threshold SOCs on renewable energy wastage (case B).

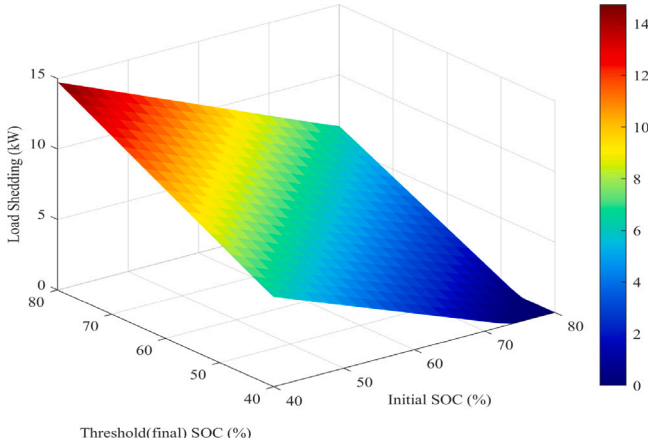

Fig. 20. Impact of initial and threshold SOCs on load shedding (case B).

in terms of load shedding and use of renewable energy resources. Therefore, impact of initial and threshold SOCs on renewable energy wastage and load shedding has been analyzed for both cases A and B. Both initial and threshold SOCs have been varied from 40% to 80% of battery capacity. The impact of initial and threshold SOCs on renewable energy wastage for case A is presented in Fig. 17. When the initial SOC is low, renewable energy waste is close to zero irrespective of threshold SOC value. However, renewable energy waste has started increasing as initial SOC becomes larger than 60%. Therefore, battery needs little charging power to reach its fully charged state and total renewable energy generation is more than total load demand that leads to higher renewable energy waste. The impact of initial and threshold SOCs on load shedding for case A is presented in Fig. 18. Load shedding does not happen in case of higher initial SOC (more than 50%) and threshold SOC of less than 70%. However, load shedding has considerably increased with low values of initial SOC (less than 50%) and threshold SOC of more than 60% due to nonavailability of enough renewable energy generation to simultaneously meet both all load demand and battery threshold SOC. Hence, both initial and threshold SOCs should be more than 50% for case A.

The impact of initial and threshold SOCs should be also be studied in case of total renewable generation to be less than total load demand. Fig. 19 shows the variation in renewable energy waste against both initial and threshold SOCs. The renewable energy waste remains constant (zero) against all values of initial and threshold SOCs as renewable energy generation is already less than total load demand. Fig. 20 presents load shedding variation with the changes in both initial and threshold SOCs. Load shedding is negligible when initial SOC is considered to be maximum and threshold SOC has lower value. However, load shedding starts increasing with the decrease in initial SOC and increase in threshold SOC. Hence, higher value of initial SOC and lower value of threshold SOC should be chosen for the case of total renewable energy generation to be less than total load demand (case B).

5. Conclusion

In this paper, a two-stage energy management system with local controllers was proposed for achieving optimized operation of an islanded DC microgrid. First stage performs optimal scheduling of distributed energy resources with the objectives of minimizing operation cost of an islanded DC MG constrained by supply demand balance, battery lifetime improvement, and maximum utilization of renewable energy sources. Second stage involves adjustment phase of decision strategies and its objective is to send the updated decision strategies to local controllers of renewable energy sources only once to reduce communication bandwidth and possibly avoid cyber attacks in real-time. The load shedding penalty cost should be set higher than battery degradation cost to avoid unnecessary load shedding. The proposed energy management system is validated by hardware-in-the-loop-based experimental setup for demonstrating its promising capability. Two cases of high and low energy generation than total load demand were considered to validate the proposed EMS performance as well as to analyze the impact and selection of initial and threshold (final) battery state of charges on renewable energy wastage and load shedding values.

The experiment results and analysis have proved the effectiveness of the proposed energy management system approach for islanded DC microgrids.

CRediT authorship contribution statement

Muhammad Fahad Zia: Conceptualization, Methodology, Simulations, Experiment, Data Analysis, Writing – original draft. **Mashood Nasir:** Methodology, Data Analysis, Experiment, Writing – original draft. **Elhoussin Elbouchikhi:** Conceptualization, Simulations, Data Analysis, Writing – review & editing. **Mohamed Benbouzid:** Conceptualization, Methodology, Data Analysis, Writing – review & editing. **Juan C. Vasquez:** Data Analysis, Writing – review & editing. **Josep M. Guerrero:** Data Analysis, Writing – review & editing.

References

[1] Chen S, Liu P, Li Z. Low carbon transition pathway of power sector with high penetration of renewable energy. Renew Sustain Energy Rev 2020;130:109985.
[2] Suberu MY, Mustafa MW, Bashir N. Energy storage systems for renewable energy power sector integration and mitigation of intermittency. Renew Sustain Energy Rev 2014;35:499–514.
[3] Saeedifard M, Graovac M, Dias RF, Iravani R. DC power systems: Challenges and opportunities. In: IEEE PES general meeting. 2010, p. 1–7.
[4] Gelani HE, Dastgeer F, Siraj K, Nasir M, Niazi KAK, Yang Y. Efficiency comparison of AC and DC distribution networks for modern residential localities. Appl Sci 2019;9(3):582.
[5] Zubieta LE. Are microgrids the future of energy?: DC microgrids from concept to demonstration to deployment. IEEE Electrif Mag 2016;4(2):37–44.
[6] Zia MF, Elbouchikhi E, Benbouzid M, Guerrero JM. Energy management system for an islanded microgrid with convex relaxation. IEEE Trans Ind Appl 2019;55(6):7175–85.
[7] Nasir M, Khan HA, Hussain A, Mateen L, Zaffar NA. Solar PV-based scalable DC microgrid for rural electrification in developing regions. IEEE Trans Sustain Energy 2018;9(1):390–9.
[8] Belila A, Benbouzid M, Berkouk E-M, Amirat Y. On energy management control of a PV-diesel-ESS based microgrid in a stand-alone context. Energies 2018;11(8):2164.
[9] Strunz K, Abbasi E, Huu DN. DC microgrid for wind and solar power integration. IEEE J Emerg Sel Top Power Electron 2014;2(1):115–26.
[10] Lu S, Wang L, Lo T-M, Prokhorov AV. Integration of wind power and wave power generation systems using a DC microgrid. IEEE Trans Ind Appl 2015;51(4):2753–61.
[11] El Tawil T, Charpentier JF, Benbouzid M. Sizing and rough optimization of a hybrid renewable-based farm in a stand-alone marine context. Renew Energy 2018;115:1134–43.
[12] Zia MF, Elbouchikhi E, Benbouzid MEH. An energy management system for hybrid energy sources-based stand-alone marine microgrid. IOP Conf Ser Earth Environ Sci 2019;322:012001.
[13] Luna AC, Diaz NL, Graells M, Vasquez JC, Guerrero JM. Mixed-integer-linear-programming-based energy management system for hybrid PV-wind-battery microgrids: Modeling, design, and experimental verification. IEEE Trans Power Electron 2017;32(4):2769–83.
[14] Zia MF, Elbouchikhi E, Benbouzid M. Microgrids energy management systems: A critical review on methods, solutions, and prospects. Appl Energy 2018;222:1033–55.
[15] Kanchev H, Lu D, Colas F, Lazarov V, Francois B. Energy management and operational planning of a microgrid with a PV-based active generator for smart grid applications. IEEE Trans Ind Electron 2011;58(10):4583–92.
[16] Daneshi H, Khorashadi-Zadeh H. Microgrid energy management system: A study of reliability and economic issues. In: 2012 IEEE power and energy society general meeting. IEEE; 2012, p. 1–5.
[17] Vasquez JC, Guerrero JM, Savaghebi M, Eloy-Garcia J, Teodorescu R. Modeling, analysis, and design of stationary-reference-frame droop-controlled parallel three-phase voltage source inverters. IEEE Trans Ind Electron 2013;60(4):1271–80.
[18] Dizqah AM, Maheri A, Busawon K, Kamjoo A. A multivariable optimal energy management strategy for standalone DC microgrids. IEEE Trans Power Syst 2015;30(5):2278–87.
[19] Boyd S, Vandenberghe L. Convex optimization. Cambridge University Press; 2004.
[20] Barelli L, Bidini G, Pelosi D, Ciupageanu D, Cardelli E, Castellini S, Lăzăroiu G. Comparative analysis of AC and DC bus configurations for flywheel-battery hess integration in residential micro-grids. Energy 2020;204:117939.
[21] Hossain MA, Pota HR, Squartini S, Zaman F, Muttaqi KM. Energy management of community microgrids considering degradation cost of battery. J Energy Storage 2019;22:257–69.
[22] Ciupageanu D-A, Barelli L, Lazaroiu G. Real-time stochastic power management strategies in hybrid renewable energy systems: A review of key applications and perspectives. Electr Power Syst Res 2020;187:106497.
[23] Maulik A, Das D. Stability constrained economic operation of islanded droop-controlled DC microgrids. IEEE Trans Sustain Energy 2019;10(2):569–78.
[24] Moayedi S, Davoudi A. Unifying distributed dynamic optimization and control of islanded DC microgrids. IEEE Trans Power Electron 2017;32(3):2329–46.
[25] Xiao J, Wang P, Setyawan L. Multilevel energy management system for hybridization of energy storages in DC microgrids. IEEE Trans Smart Grid 2016;7(2):847–56.
[26] Sen S, Kumar V. Simplified modeling and hil validation of solar pvs and storage-based islanded microgrid with generation uncertainties. IEEE Syst J 2019;1–12. http://dx.doi.org/10.1109/JSYST.2019.2917754.
[27] Yin C, Wu H, Locment F, Sechilariu M. Energy management of DC microgrid based on photovoltaic combined with diesel generator and supercapacitor. Energy Convers Manage 2017;132:14–27.
[28] Han Y, Chen W, Li Q, Yang H, Zare F, Zheng Y. Two-level energy management strategy for PV-fuel cell-battery-based DC microgrid. Int J Hydrogen Energy 2019;44(35):19395–404.
[29] Michaelson D, Mahmood H, Jiang J. A predictive energy management system using pre-emptive load shedding for islanded photovoltaic microgrids. IEEE Trans Ind Electron 2017;64(7):5440–8.
[30] Pu Y, Li Q, Chen W, Liu H. Hierarchical energy management control for islanding DC microgrid with electric-hydrogen hybrid storage system. Int J Hydrogen Energy 2019;44(11):5153–61.
[31] Han Y, Zhang G, Li Q, You Z, Chen W, Liu H. Hierarchical energy management for PV/hydrogen/battery island DC microgrid. Int J Hydrogen Energy 2019;44(11):5507–16.
[32] Zia MF, Nasir M, Elbouchikhi E, Benbouzid M, Vasquez JC, Guerrero JM. Energy management system for an islanded renewables-based DC microgrid. In: 2020 2nd international conference on smart power internet energy systems (SPIES). 2020, p. 543–7.
[33] Sioshansi R, Conejo AJ. Optimization in engineering. Springer International Publishing; 2017.
[34] Zia MF, Elbouchikhi E, Benbouzid M. Optimal operational planning of scalable DC microgrid with demand response, islanding, and battery degradation cost considerations. Appl Energy 2019;237:695–707.
[35] Lofberg J. Yalmip : a toolbox for modeling and optimization in matlab. In: 2004 IEEE international conference on robotics and automation (IEEE Cat. No. 04CH37508). 2004, p. 284–9.
[36] Ngan MS, Tan CW. A study of maximum power point tracking algorithms for stand-alone photovoltaic systems. In: 2011 IEEE applied power electronics colloquium (IAPEC). IEEE; 2011, p. 22–7.
[37] Abbasi MA, Zia MF. Novel TPPO based maximum power point method for photovoltaic system. Adv Electr Comput Eng 2017;17(3):95–100.
[38] Patsios C, Chaniotis A, Rotas M, Kladas A. A comparison of maximum-power-point tracking control techniques for low-power variable-speed wind generators. In: 2009 8th international symposium on advanced electromechanical motion systems & electric drives joint symposium. IEEE; 2009, p. 1–6.
[39] Zhou Z, Ben Elghali S, Benbouzid M, Amirat Y, Elbouchikhi E, Feld G. Tidal stream turbine control: An active disturbance rejection control approach. Ocean Eng 2020;202:107190.
[40] Oliveira TR, Silva WWAG, Donoso-Garcia PF. Distributed secondary level control for energy storage management in DC microgrids. IEEE Trans Smart Grid 2017;8(6):2597–607.
[41] Nasir M, Jin Z, Khan HA, Zaffar NA, Vasquez JC, Guerrero JM. A decentralized control architecture applied to DC nanogrid clusters for rural electrification in developing regions. IEEE Trans Power Electron 2019;34(2):1773–85.
[42] Erickson RW, Maksimović D. Fundamentals of power electronics. Springer US; 2001.
[43] Luna AC, Meng L, Diaz NL, Graells M, Vasquez JC, Guerrero JM. Online energy management systems for microgrids: Experimental validation and assessment framework. IEEE Trans Power Electron 2018;33(3):2201–15.